

## Virial coefficients and inversion curve of simple and associating fluids

D.J. Naresh, Jayant K. Singh\*

Department of Chemical Engineering, Indian Institute of Technology Kanpur, Kanpur, UP 208016, India

### ARTICLE INFO

#### Article history:

Received 23 October 2008

Received in revised form 5 January 2009

Accepted 26 January 2009

Available online 7 February 2009

#### Keywords:

Mayer sampling

Virial coefficient

Joule–Thomson coefficient

Boyle temperature

### ABSTRACT

Free energy simulation method is applied to calculate the virial coefficients of square-well (SW) fluids of variable well-width and square-well based dimer forming associating fluids. In this approach, Monte Carlo sampling is performed on a number of molecules equal to the order of integral, and configurations are weighted according to the absolute value of the integrand. An umbrella-sampling average yields the value of the cluster integral in reference to a known integral. By using this technique, we determine the virial coefficients up to  $B_6$  for SW fluid with variable potential range from  $\lambda = 1.25$  to  $\lambda = 3.0$  and model associating fluids with different association strengths:  $\varepsilon_{af} = 0.0, 8.0, 16.0$  and  $22.0$ . These calculated values for SW fluids are in good agreement with the literature. We examine these coefficients in the context of the virial equation of state (VEOS) of SW fluids. VEOS up to  $B_4$  or up to  $B_6$  describes the PVT behavior along the saturated vapor line better than the series that includes  $B_5$ . We used these coefficients to find the critical properties of SW fluids and compared with the literature values. Boyle temperature is also determined and is found to increase with the increase in the well-extent and associating strength. We also report Joule–Thomson inversion curve for Lennard–Jones fluid and SW fluids using different truncated VEOS and compared with that predicted from established EOS.

© 2009 Elsevier B.V. All rights reserved.

### 1. Introduction

The equation of state of real gas can be expressed as a power series, as a function of density, with temperature dependent coefficients due to statistical mechanical route and expressed by:

$$\frac{P}{\rho kT} \equiv Z = 1 + B_2\rho + B_3\rho^2 + B_4\rho^3 + B_5\rho^4 + B_6\rho^5 + \dots \quad (1)$$

where  $P$  is the pressure,  $\rho$  is the number density,  $k$  is the Boltzmann constant,  $T$  is the absolute temperature,  $Z$  is the compressibility factor, and  $B_i$  is the  $i$ th virial coefficient. Eq. (1) is also widely known as virial equation of state (VEOS).

The theoretical importance of the virial expansion [1] is well known through statistical thermodynamics [2,3]. An attractive feature of virial expansion is that the virial coefficients are given exactly in terms of cluster integrals involving the intermolecular potential between particles [4]. The thermodynamic properties of gases may be easily calculated from the knowledge of the virial coefficients and their dependence on temperature. The virial expansion has found applications in various applications for example, in the development of natural gas equation of state [5] and in the calculation of activity coefficients in the vapor–liquid equilibria [6]. The second virial coefficient provides information about intermolecu-

lar interactions between a pair of molecules. Similarly, the third and fourth virial coefficients represent deviations from ideal behavior when collisions involving three and four molecules become important. Consequently, at low gas densities, deviations from ideality are adequately described by the second virial coefficient, whereas at higher densities higher virial coefficients must be included. These forces between molecules are of interest to scientists in a wide range of disciplines as these interactions control the progress of molecular collisions and determine the bulk properties of matter. Virial coefficients of real systems can be measured experimentally by a number of different techniques such as PVT measurements [7], speed of sound measurements [8], Joule–Thomson measurements and self-interaction chromatography [9]. Various correlations have been developed to calculate the second and third virial coefficients. For example, recently Meng et al. [10,11] presented an empirical correlation for the second and third virial coefficients of polar fluids such as ammonia, water, acetone, ethanol and associating fluids such as methanol, propanol, butanol and quantum fluids based on the principle of the corresponding states.

In last few decades computer simulation has become a major and very successful tool in the understanding of the phase diagram and structural properties of simple [12–15] and complex fluids such as polymers [16], and colloidal systems [17]. Development of EOS based on perturbation theories has also been done rigorously. For example, EOS for Lennard–Jones [18,19], square-well and associating fluids [20,21] are well known. However, EOS based on cluster integral, which appears in the statistical mechanics, is not being

\* Corresponding author.

E-mail address: [jayantks@iitk.ac.in](mailto:jayantks@iitk.ac.in) (J.K. Singh).

extensively developed mainly due to the difficulty in calculating cluster integral of higher order and for complex molecules. Virial coefficient data for realistic potentials are scarce. Recently, Kofke and co-workers introduced Mayer sampling and its variants, which are based on free energy perturbation techniques for the calculation of cluster integrals [22–25]. Using this method, virial coefficient up to  $B_6$  for Lennard–Jones fluid (LJ) [22,23] and a host of pair-wise water models were calculated [25]. Additionally, virial coefficients up to  $B_4$  for two-centered Lennard–Jones with quadrupole (2CLJQ) [26] and  $B_3$  for the polarizable point charge (PPC) water model [27] have been determined using other methodologies, such as numerical integration and the hit-and-miss Monte Carlo (MC) method.

In the present study, we have applied the Mayer sampling method to investigate the long range behavior of potential and short range directional interaction, as found in the associating fluid, on virial coefficient  $B_2$ – $B_6$  and subsequently various different analysis has been done using viral EOS for obtaining critical properties, Joule–Thomson coefficient and inversion curve. In order to understand the effect of long-range interaction on the virial coefficient, we have chosen SW potential, which is given by:

$$u(r_{ij}) = \begin{cases} \infty, & 0 < r_{ij} < \sigma, \\ -\varepsilon, & \sigma \leq r_{ij} < \lambda\sigma, \\ 0, & \lambda\sigma \leq r_{ij}, \end{cases} \quad (2)$$

where  $r_{ij}$  is the distance between two particles,  $\sigma$  is the diameter of the hard-core repulsive interaction,  $\lambda\sigma$  is the well extent, and  $\varepsilon$  is the depth of the isotropic well.

SW fluid has both repulsive and attractive forces, so it has been chosen as a reference system in many theoretical models [12–15]. Due to its importance, the thermodynamic properties of square-well fluid have been studied using computer simulation methods in both the one phase region [28–31] and the two-phase region [13,32,33]. There has also been a considerable work done to obtain an EOS for a variable-width square-well fluids [28,32,34,35]. Square-well model has been taken by few researchers [36–38] to model associating fluids such as water and hydrogen fluoride (HF). Strongly associating fluids are an important class of systems featuring intermolecular attractions with deep, but narrow wells usually caused by the formation of intermolecular hydrogen bonds. These fluids find importance in various industrial processes such as chromatography, heterogeneous catalyst reactions, oil recovery, gas storage, membrane separation, and lubricant processes. In this work, we have used the following potential to model associating fluids:

$$u(r_{ij}, \theta_i, \theta_j) = \begin{cases} \infty, & 0 < r_{ij} < \sigma, \\ u_{af}, & \sigma \leq r_{ij} < r_c\sigma, \\ -\varepsilon, & r_c\sigma \leq r_{ij} < \lambda\sigma, \\ 0, & r_{ij} \geq \lambda\sigma. \end{cases} \quad u_{af}(r_{ij}, \theta_i, \theta_j) = \begin{cases} -\varepsilon_{af}, & \text{if } \theta_i < \theta_c \text{ and } \theta_j < \theta_c, \\ -\varepsilon, & \text{otherwise,} \end{cases} \quad (3)$$

where  $\theta_i$  and  $\theta_j$  are angles between the center-to-center vector and the direction vectors on the respective atoms  $i$  and  $j$ , and  $\varepsilon_{af}$  is the well depth of the association cone. In this study, for associating model we use  $\theta_c = 27^\circ$ ,  $\lambda = 1.5$  and  $r_c = 1.05$ . We adopt units such that  $\varepsilon$  and  $\sigma$  are unity. Reduced units used in this study are temperature  $T^* = kT/\varepsilon$ , density  $\rho^* = \rho\sigma^3$ , pressure  $P^* = P\sigma^3/\varepsilon$  and virial coefficients  $B_i^* = B_i/b^{i-1}$ , where  $B_i$  is the  $i$ th virial coefficient and  $b = 2\pi\sigma^3/3$  is the second virial coefficient of the hard-sphere.

The rest of the paper is organized as follows. Section 2 presents a brief introduction of the methodology used in this work along with the simulation details. The results are systematically discussed in Section 3, which is followed by a summary in Section 4.

## 2. Methodology

In this paper, we use Mayer sampling technique [22], which is described by Kofke and co-workers in detail [25]. We briefly illustrate the methodology. The method is based on performing molecular simulation on the molecules represented in the cluster integral appearing in the statistical mechanical formulation of virial coefficients. There are two key ideas in its application to cluster integrals. First, we generate configurations of molecules using Metropolis MC [39] with importance sampling based on the magnitude of the interactions represented in the cluster integral. Second, we need to evaluate the ratio of the desired cluster integral to a known reference integral. We do not attempt to evaluate the cluster integral directly. The umbrella sampling method provides one such formula

$$\Gamma(T) = \Gamma_0 \frac{\Gamma}{\Gamma_0} = \Gamma_0 \frac{\langle \gamma/\pi \rangle_\pi}{\langle \gamma_0/\pi \rangle_\pi}. \quad (4)$$

In the above expression,  $\Gamma(T)$  represents a cluster integral or sum of integrals with integrand  $\gamma(r^n; T)$ . The angle brackets indicate the “ensemble average” integral over all configurations and orientations of the  $n$  molecules, and the subscript  $\pi$  indicates that the integral is weighted by the normalized  $\pi$  distribution. The subscript ‘0’ indicates a quantity for a reference system, for which  $\Gamma_0$  is known. The method involves perturbations directly between the target system (which governs sampling) and the reference system.

There are many choices one can select for the  $\pi$  distribution and the reference cluster [22]. In this work we have used  $\pi = |\gamma(r^n; T)|$ , as suggested by the importance sampling approach. We use  $\pi$  as the absolute value of the sum of all clusters. By choosing this definition for  $\pi$ , Eq. (4) can be expressed as

$$\Gamma(T) = \Gamma_0 \frac{\langle \text{sgn}(\gamma) \rangle_\pi}{\langle \gamma_0/\pi \rangle_\pi}, \quad (5)$$

where  $\text{sgn}(\gamma)$  is just the sign of the cluster sum. Therefore, each term in numerator average is +1 or –1.

Regarding the reference cluster one must select a system whose phase space is a subset of the phase space of the target system [40,41]. In this work, we use the ring-shaped cluster with a hard-sphere potential as a reference for sampling simulations.

We have applied the methodology described here to evaluate the second to sixth virial coefficients of square-well fluids and one-site associating fluids. The calculations were conducted as follows. MC sampling was performed for a number of molecules equal to the order of the virial coefficient being computed. Trial configurations were generated using molecular displacement MC move and cluster MC moves [22] for square well fluids. In addition to the aforementioned MC moves, for associating fluids, we have also

used rotation move. Each trial was accepted with probability  $\min(1, \pi^{\text{new}}/\pi^{\text{old}})$ , where  $\pi$  is defined as the absolute value of the weighted sum of the cluster integrands contributing to the calculated virial coefficient. The value of a cluster for a given configuration was determined by summing the contributions of all unique permutations of the labeling of the molecules. In this work,  $10^9$  configurations were generated for the estimation of virial coefficients. Step sizes for the trials were adjusted in a short “equilibration” period, before accumulating averages, to achieve a 50% acceptance rate for trial moves.

Virial coefficients up to  $B_4$  for the square-well and associating fluids are easily done on a single core of quad core processor

within 2 h. For higher-order coefficients ( $B_5$  and  $B_6$ ), longer runs are required to collect the required number of configurations. For example, calculating  $B_5$  at a given temperature required 60–65 h on a single core of quad core 2.66 GHz processor to generate  $10^9$  configurations. Four independent runs were conducted to calculate the statistical error. All simulations in this work were performed with the Etonica molecular simulation suite [42].

### 3. Results and discussion

We have carried out Mayer sampling (MS) based MC simulations to calculate virial coefficients up to  $B_6$  for SW fluid of well widths  $\lambda = 1.25, 1.5, 1.75, 2.0,$  and  $3.0$  and dimer-forming associating fluid of various association strengths  $\varepsilon_{af} = 0.0, 8.0, 16.0,$  and  $22.0$ . We start our discussion with the results of SW fluids. Fig. 1 presents a plot of  $B_2^*$  as a function of temperature for SW fluids of different well extents. In all the cases, we observed  $B_2^*$  to be negative at subcritical temperature. Increase in temperature increases the  $B_2^*$  and it becomes positive at high temperature. This trend is similar to that observed for LJ fluid [22]. At a particular temperature the value of  $B_2^*$  decreases with the increase in the well-extent. Consequently, the temperature at which  $B_2 = 0$  (Boyle temperature) increases as the well-extent increases. Computed  $B_2^*$  values, in this work, are compared with the literature data [34] and found to be in good agreement. Fig. 2 presents a plot of  $B_3^*$  as a function of temperature for SW fluids of various well extents.  $B_3^*$  is observed to be negative at subcritical temperature similar to the behavior seen for  $B_2^*$ . For lower well width viz.,  $\lambda = 1.25$  and  $1.5$ , we observed an increase in the third virial coefficient with the increase in the temperature.  $B_3^*$  reaches a maximum and subsequently it slowly decreases until a minimum is obtained. Further increase in the temperature increases  $B_3^*$  albeit not dramatic and eventually the values are indifferent to the change of temperature. Such behavior is also visible for fluid of well extent  $\lambda = 1.75$ , although not distinctly. At higher well width, we observed a similar behavior as seen for LJ fluids [22], i.e., after the first maximum, with the increase in the temperature,  $B_3^*$  gradually decrease. The peak or the maximum value of  $B_3^*$  increases with the well extent up to  $2.0$  and subsequently it decreases as clearly visible for  $\lambda = 3.0$ . The temperature at which the maximum of  $B_3^*$  is attained does depend on the well-extent and is found to increase with the well extent.  $B_3^*$ 's computed in this work are in good agreement with the literature data [34].

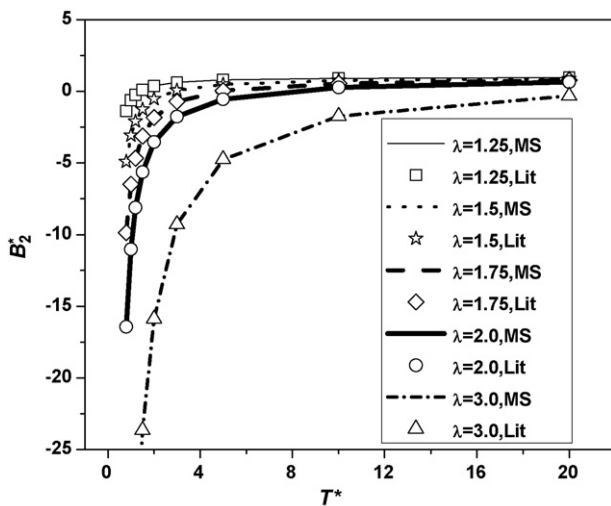


Fig. 1. Temperature dependence of  $B_2^*$  of SW fluids at  $\lambda = 1.25, 1.5, 1.75, 2.0,$  and  $3.0$ . Lines represent the current estimated value and symbols correspond to literature data [34].

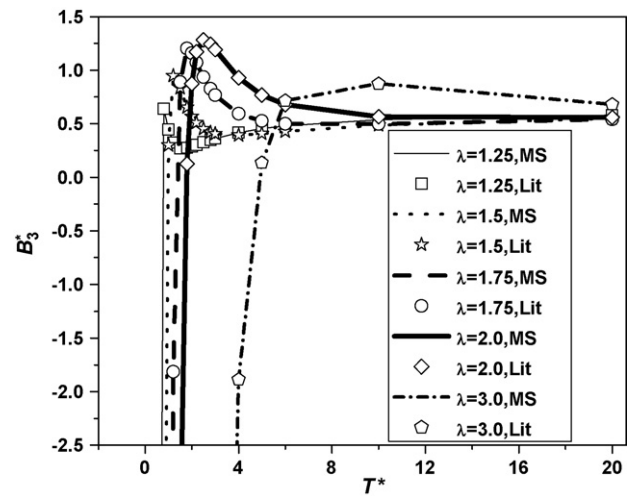


Fig. 2. Temperature dependence of  $B_3^*$  of SW fluids at  $\lambda = 1.25, 1.5, 1.75, 2.0,$  and  $3.0$ . Lines represent the current estimated value and symbols correspond to literature data [34].

In Fig. 3, we plot  $B_4^*$  as a function of temperature for SW fluids of different well extents. The observed trends are qualitatively similar to those observed for  $B_3^*$ . The behavior of  $B_4^*$  of SW fluids is similar to that of LJ fluid [22] with the exception of  $\lambda = 3.0$ , where no peak was observed. Mayer sampling values are compared with literature data [43,44], at well extents  $\lambda = 1.5$  and  $2.0$ , and found to be in good agreement.

$B_5^*$  for LJ fluid [22] is known to increase sharply from large negative value towards a small positive value with increase in the temperature until a maximum is attained. Subsequent increase in temperature led to first decrease  $B_5^*$  to sub-zero minimum value and then increase again to attain another maximum value higher than the first one. Further increase in the temperature decreases the coefficient values although gradually and eventually  $B_5^*$  does not significantly change with the change in the temperature.  $B_5^*$  of SW fluids surprisingly (see Fig. 4) do not contain substantial oscillatory behavior as seen for LJ fluid. Instead, we observed only a small kink of  $B_5^*$  value before continuously increasing towards a small but positive value at higher temperature. The behavior of  $\lambda = 3.0$  is once again quite different from smaller well extents and  $B_5^*$  for this fluid continuously increases with increasing temperature however,

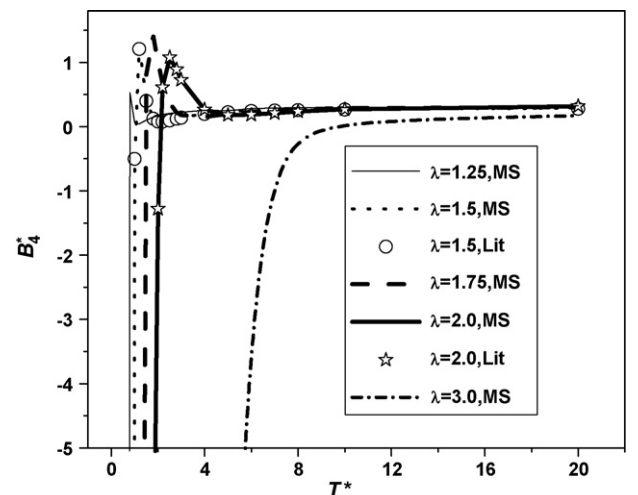
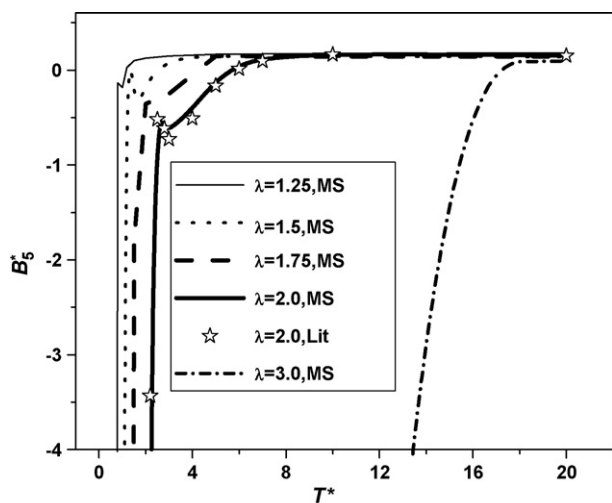


Fig. 3. Temperature dependence of  $B_4^*$  of SW fluids at  $\lambda = 1.25, 1.5, 1.75, 2.0,$  and  $3.0$ . Lines correspond to Mayer sampling results and symbols represent literature values [43].

**Table 1**  
Sixth virial coefficient,  $B_6^* = B_6/b^5$  of square-well fluids of variable well extents,  $\lambda$ .

$T^*$	$\lambda = 1.25$	$\lambda = 1.5$	$\lambda = 1.75$	$\lambda = 2.0$	$\lambda = 3.0$
0.8	-0.8415(22)	-23382(215)			
1.0	-0.0239(4)	-73(1)	-59318(354)		
1.2	0.0481(1)	-3.823(2)	-3136(16)	-157920(310)	
1.5	0.0299(5)	-0.685(3)	-47.8(7)	-10556(152)	
2.0	0.0341(1)	0.163(4)	-3.326(18)	-145(2)	-1245325(6588)
3.0	0.0381(2)	0.085(3)	0.1279(16)	-1.66(3)	-313025(4116)
5.0	0.0396(1)	0.0623(5)	0.1369(4)	0.215(1)	-727(13)
10	0.0398(1)	0.0526(1)	0.0687(1)	0.0957(4)	0.407(3)
20	0.0394(1)	0.0459(1)	0.0499(1)	0.0447(1)	0.1455(1)

Numbers in parentheses indicate the 67% confidence limits of the last digit of the reported value.



**Fig. 4.** Temperature dependence of  $B_6^*$  of SW fluids at  $\lambda = 1.25, 1.5, 1.75, 2.0,$  and  $3.0$ . Comparison is made with the available literature data for  $\lambda = 2.0$ . Lines correspond to Mayer sampling results and symbols represent literature values [45].

at higher temperature it also attain a positive but small value. Computed values are compared with the available literature data [45], for well extent  $\lambda = 2.0$ , and found to be in good agreement.

The sixth virial coefficients,  $B_6^*$ 's, for SW fluids of different well extents are calculated for the first time. The results are recorded in Table 1. Fig. 5 presents the  $B_6^*$  as a function of temperature for SW fluids at different well extents. The observed trends are qualitatively similar to those observed for LJ fluid [22]. Long-range attraction

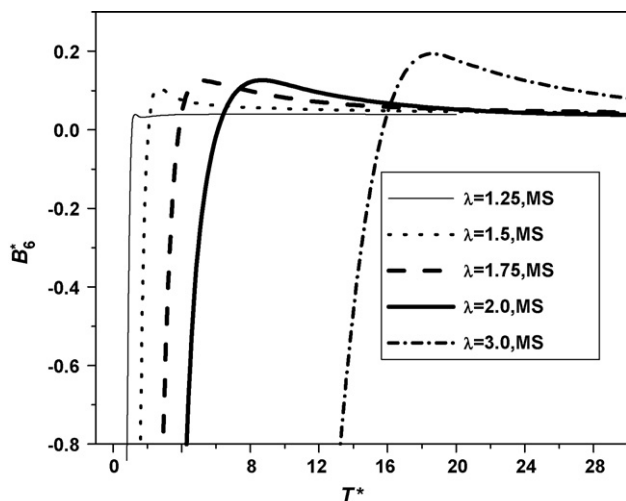


**Fig. 5.** Temperature dependence of the virial coefficient  $B_6^*$  of SW fluids at  $\lambda = 1.25, 1.5, 1.75, 2.0,$  and  $3.0$ .

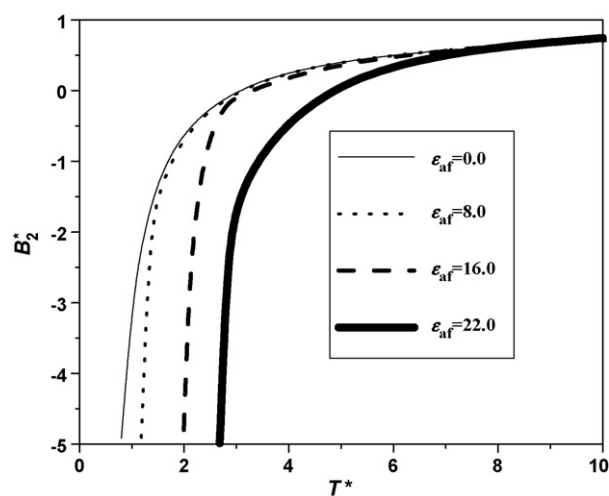


**Fig. 6.** Temperature dependence of  $B_2^*$  of associating fluid at  $\lambda = 1.5$  with different association strengths,  $\epsilon_{af} = 0.0, 8.0, 16.0,$  and  $22.0$ .

tends to shift the curve towards higher temperature. It is interesting to observe that all the calculated virial coefficients fall on one master curve in a corresponding plot,  $B_i^* \rho_c^i$  vs.  $T/T_c$  (figure not shown), where  $B_i^*$ ,  $T_c^*$  and  $\rho_c^*$  are the  $i$ th virial coefficient, critical temperature and critical density, respectively.

Figs. 6–10 present the virial coefficients for dimer-forming associating fluids of variable association strengths. Fig. 6 presents  $B_2^*$ 's at association strengths  $\epsilon_{af} = 0.0, 8.0, 16.0,$  and  $22.0$  as a function of temperature. These values are calculated at well-extent,  $\lambda = 1.5$ . The

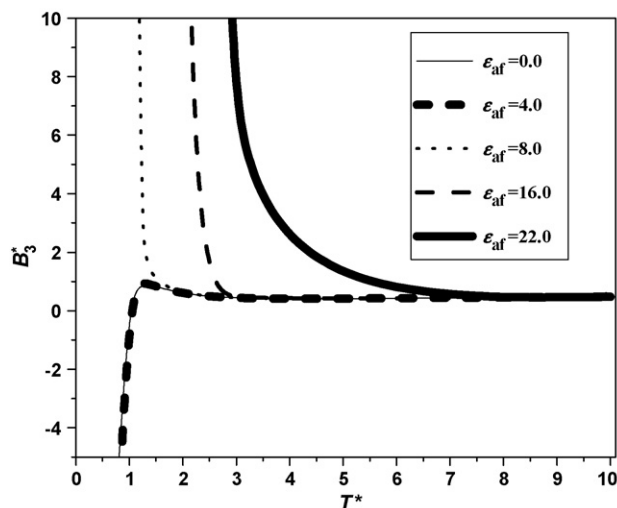


**Fig. 7.** Temperature dependence of  $B_3^*$  of associating fluid at  $\lambda = 1.5$  with different association strengths,  $\epsilon_{af} = 0.0, 4.0, 8.0, 16.0,$  and  $22.0$ .

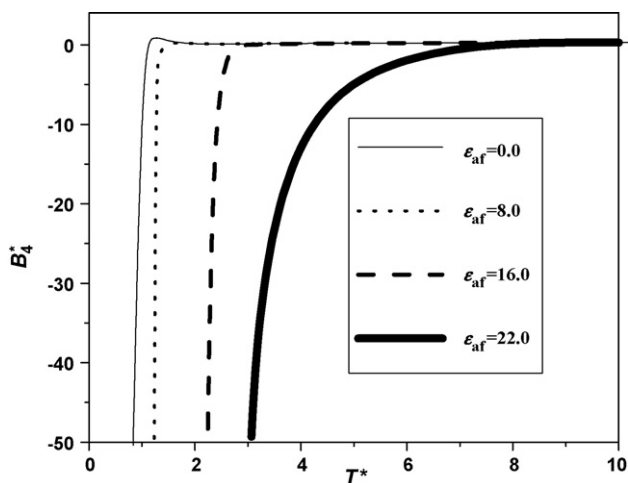


Fig. 8. Temperature dependence of  $B_4^*$  of associating fluid at  $\lambda = 1.5$  with different association strengths,  $\epsilon_{af} = 0.0, 8.0, 16.0,$  and  $22.0$ .

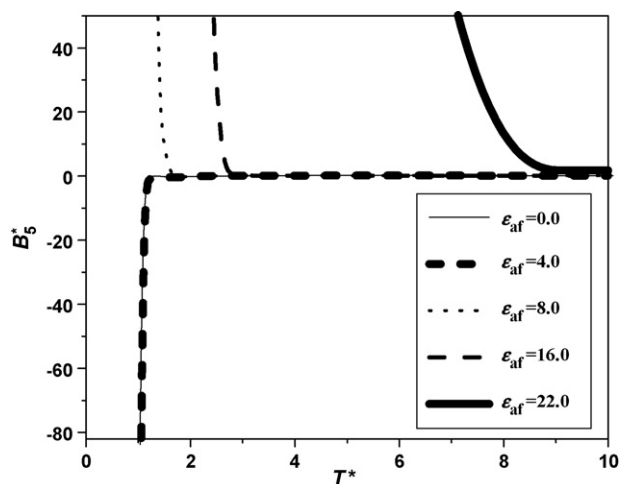


Fig. 9. Temperature dependence of  $B_5^*$  of associating fluid at  $\lambda = 1.5$  with different association strengths,  $\epsilon_{af} = 0.0, 4.0, 8.0, 16.0,$  and  $22.0$ .

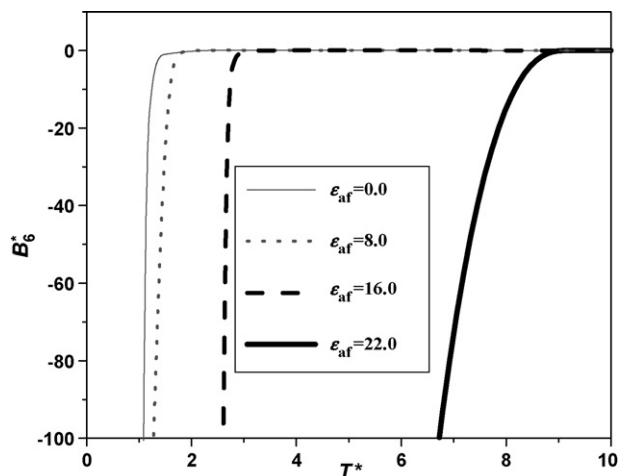


Fig. 10. Temperature dependence of  $B_6^*$  of associating fluid at  $\lambda = 1.5$  with different association strengths,  $\epsilon_{af} = 0.0, 8.0, 16.0,$  and  $22.0$ .

behavior is akin to SW fluids and water [22].  $B_3^*$  on the other hand behaves differently for different association energy, as depicted in Fig. 7. For weak associating strength,  $\epsilon_{af} = 4.0$ ,  $B_3^*$  is seen to be negative at low temperature. Subsequently, it increases to a maximum and gradually decreases with the increase in the temperature, similar to the case of non-associating fluid,  $\epsilon_{af} = 0.0$ , and water [22]. Surprisingly at higher association strength  $B_3^*$  behaves completely different from that seen at lower association strength. At association strengths  $\epsilon_{af} = 8.0, 16.0$  and  $22.0$ ,  $B_3^*$  is seen to be large positive value at lower temperatures and continuously decreases to a small positive value at higher temperatures.

In Fig. 8, we plot  $B_4^*$  as a function of temperature for model associating fluids with different association strengths. We observed very low values of  $B_4^*$  for  $\epsilon_{af} > 0$  and it increases towards a positive value, sharply at lower association strengths and smoothly at higher association strengths, with the increase in the temperature.  $B_5^*$  of associating fluids is akin to  $B_3^*$  i.e., for lower associating strength,  $B_5^*$  increases from a negative value towards a small positive value. With the increase in the associating strength  $B_5^*$  jumps to a high positive value, at low temperature, and decrease towards a small positive value with the increase in the temperature.  $B_6^*$ , as presented in Fig. 9, on the other hand has the generic behavior for all the associating strength studied in this work similar to  $B_2^*$ .

### 3.1. Critical properties

In this section, we present critical properties; temperature  $T_c^*$ , density  $\rho_c^*$  and pressure  $P_c^*$  of square-well fluid at well extents  $\lambda = 1.25, 1.5, 1.75, 2.0,$  and  $3.0$ , and one site associating fluids with different association strengths, estimated using the third (VEOS3), fourth (VEOS4) and fifth (VEOS5) order truncated virial EOS and compared with literature values. These critical properties are determined from the following thermodynamic conditions:

$$\left(\frac{\partial p}{\partial V}\right)_{T_c} = 0, \quad \left(\frac{\partial^2 p}{\partial V^2}\right)_{T_c} = 0. \quad (6)$$

Table 2 records all the estimated critical properties based on different truncated series. The literature value of estimated critical temperature of SW fluids substantially varies. In this work, we have taken  $T_c^* = 0.536, 1.217, 1.809, 2.68$  and  $9.871$  as the critical temperature for  $\lambda = 1.25, 1.5, 1.75, 2.0$  and  $3.0$ , respectively for comparison. These values were taken due to their reasonable agreement with some recent work on critical properties of SW fluids. The performance of truncated VEOS for the estimation of critical temperature fluctuates with the well extents. For smaller interaction range, values of VEOS3 and VEOS4 are closer to the literature data; however the deviation from the literature data is non-negligible. Addition of  $B_5$  further increases the deviation from the literature data. At well extent  $\lambda = 1.5$ , the estimated critical properties by the truncated third order VEOS fall within 10% of literature data; however, critical pressure is highly overestimated (40%) by VEOS3. On the other hand, VEOS4 predicts critical temperature and pressure within 5% and 20% of the literature data, respectively; however, critical density is underestimated by 41%. With the addition of fifth virial coefficient,  $T_c^*$  slightly decreases but  $B_5^*$  significantly diminishes critical density and pressure. Similar behavior is seen for  $\lambda = 1.75$ . For higher well extents,  $\lambda = 2.0$ , addition of  $B_5^*$  on the contrary increase the critical properties. In summary, VEOS3 appears to be a suitable formalism among all the truncated VEOS studied in this work due to the reasonable prediction of all the critical properties for square-well fluids with well extent higher than 1.25. VEOS4, on the other hand, is most appropriate for the prediction of critical temperature whereas VEOS5 is relatively unsuitable form of virial EOS for the prediction of critical properties. It is worth noting that it is extremely hard to calculate accurate virial coefficients near the

**Table 2**

The critical temperature  $T_c^*$ , density  $\rho_c^*$  and pressure  $P_c^*$  of square-well fluids of variable potential range  $\lambda$  estimated from virial equation of state and compared with literature values.

$\lambda$	$T_c^*$	$\rho_c^*$	$P_c^*$	Source	
1.25	0.7978(2)	0.3447(3)	0.0913(1)	This work (VEOS3)	
	0.765(3)	0.1715(9)	0.0744(3)	This work (VEOS4)	
	1.064(10)	0.284(2)	0.3295(8)	This work (VEOS5)	
	0.913	0.34	0.1333	Henderson et al. <sup>g</sup>	
	0.850	0.48	0.189	Chang et al. <sup>h</sup>	
	0.536	0.4717	0.0739	Elliot et al. <sup>a</sup>	
1.5	1.3239(7)	0.2842(3)	0.1254(2)	This work (VEOS3)	
	1.166(1)	0.183(1)	0.0764(3)	This work (VEOS4)	
	1.137(14)	0.154(4)	0.047(2)	This work (VEOS5)	
	1.33	0.29	0.146	Henderson et al. <sup>g</sup>	
	1.35	0.31	0.15	Chang et al. <sup>h</sup>	
	1.2	0.196	0.0665	Guo et al. <sup>i</sup>	
	1.27	0.305577	0.11	Elliot et al. <sup>a</sup>	
	1.2172	0.3079	0.0931	Singh et al. <sup>b</sup>	
	1.218	0.310	0.095	Orkoulas et al. <sup>c</sup>	
	1.218	0.3016	0.0939	Del Rio et al. <sup>d</sup>	
	1.219	0.299	0.108	Vega et al. <sup>e</sup>	
	1.75	1.9776(6)	0.2555(1)	0.1684(1)	This work (VEOS3)
		1.723(4)	0.169(1)	0.1041(7)	This work (VEOS4)
1.707(15)		0.156(5)	0.096(4)	This work (VEOS5)	
1.93		0.24	0.1667	Henderson et al. <sup>g</sup>	
2.04		0.25	0.1938	Chang et al. <sup>h</sup>	
1.79		0.26738	0.12	Elliot et al. <sup>a</sup>	
1.809		0.2653	0.1263	Singh et al. <sup>b</sup>	
1.808		0.2648	0.1276	Del Rio et al. <sup>d</sup>	
1.811		0.284	0.179	Vega et al. <sup>e</sup>	
2.0		2.844(33)	0.245(5)	0.232(7)	This work (VEOS3)
	2.559(32)	0.177(5)	0.157(6)	This work (VEOS4)	
	2.614(31)	0.202(9)	0.172(3)	This work (VEOS5)	
	2.79	0.2253	0.22	Chang et al. <sup>h</sup>	
	2.61	0.26738	0.17	Elliot et al. <sup>a</sup>	
	2.68	0.251	0.1975	Singh et al. <sup>b</sup>	
	2.691	0.2549	0.2021	Del Rio et al. <sup>d</sup>	
	2.764	0.225	0.197	Vega et al. <sup>e</sup>	
	3.0	9.786(15)	0.264(3)	0.869(10)	This work (VEOS3)
9.83(13)		0.0047(1)	0.046(1)	This work (VEOS4)	
9.871		0.2578	0.841	Orkoulas et al. <sup>c</sup>	
9.961		0.254	0.889	Kiselev et al. <sup>f</sup>	

Numbers in parentheses indicate the 67% confidence limits of the last digit of the reported value.

<sup>a</sup> Ref. [32].

<sup>b</sup> Ref. [12].

<sup>c</sup> Ref. [33].

<sup>d</sup> Ref. [61].

<sup>e</sup> Ref. [13].

<sup>f</sup> Ref. [34].

<sup>g</sup> Ref. [28].

<sup>h</sup> Ref. [62].

<sup>i</sup> Ref. [29].

critical temperature due to the high degree of cancellation between the Ree–Hoover graphs. Further, the nature of the oscillation of virial coefficients makes VEOS extremely difficult to converge particularly within six coefficients hence, reasonable critical property prediction by VEOS3 and VEOS4 appears to be fortuitous.

**Table 3**

The critical temperature  $T_c^*$ , density  $\rho_c^*$  and pressure  $P_c^*$  data of associating fluids with well extent  $\lambda = 1.5$  for variable associating strengths,  $\varepsilon_{af}$ , estimated from VEOS3.

$\varepsilon_{af}$	$T_c^*$	$\rho_c^*$	$P_c^*$
0.0	1.324(1)	0.284(1)	0.125(1)
8.0	1.343(7)	0.315(10)	0.413(8)
16.0	3.575(9)	0.351(8)	1.239(14)
22.0	5.306(18)	0.318(4)	1.693(21)

Numbers in parentheses indicate the 67% confidence limits of the last digit of the reported value.

**Table 4**

Boyle temperature,  $T_B^*$ , of square-well fluids of variable well extent and associating fluids with well extent,  $\lambda = 1.5$ .

$\lambda$	$T_B^*$	$\varepsilon_{af}$	$T_B^*$
1.25	1.41	0.0	2.94
1.5	2.94	8.0	2.97
1.75	4.97	16.0	4.94
2.0	9.77	22.0	4.99
3.0	49.3		

Table 3 presents the estimated critical temperature using VEOS3 for dimer-forming associating fluids. As expected, critical temperature is found to increase with the increase of the associating strength.

### 3.2. Boyle temperature

Boyle temperature is defined as the temperature where  $B_2(T^* = T_B^*) = 0$ . Usually,  $T_B^*$  is much higher than the corresponding critical temperature; hence experimentally the calculation of Boyle temperature is generally not feasible. On the other hand, EOS provides an easy mean for the calculation of Boyle temperature. Menduina et al. [46] and MacDowell et al. [26] determined the Boyle temperatures for the dipolar and quadrupolar two center Lennard–Jones models and found that it decreases with the reduced bond length and increases with the reduced dipole moment and quadrupole moment. Recently, Estrada-Torres and co-workers [47] used a semi-empirical EOS to find Boyle temperature for numerous pure substances. Most of Boyle temperatures estimated are in the range of  $2.13T_c^*$  to  $3.35T_c^*$ , with the exception of  $\text{CO}_2$ , He and CO for which  $T_B/T_c = 5.4, 4.34$  and  $1.12$ , respectively. We have calculated  $T_B^*$  for SW and associating fluids and the values are tabulated in Table 4. Fig. 11 presents a plot of reduced Boyle temperature,  $T_B/T_c$ , for SW fluids. The reduced Boyle temperature is found to increase almost linearly with the increase in the well extent. We also observed Boyle temperature to increase with the increase in the association strength. It is noteworthy that  $T_B^*$  is found to be more sensitive to the interaction range compared to the strength of association. For moderate association range, the reduced Boyle temperature is in the same range for the non-associating fluid. However, at higher association strength the reduced Boyle temperature decreases (see Table 4). This is also reported in Estrada-Torres and co-worker's recent work [47], where the reduced Boyle temperature for water, 2.47, was found to be lower than that for methane, 2.67.

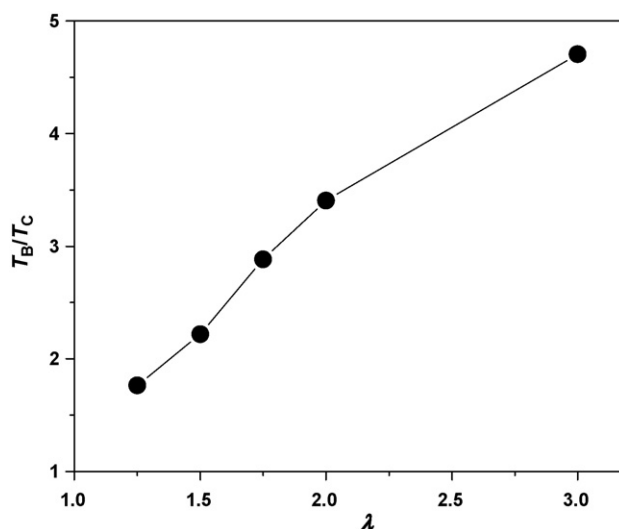
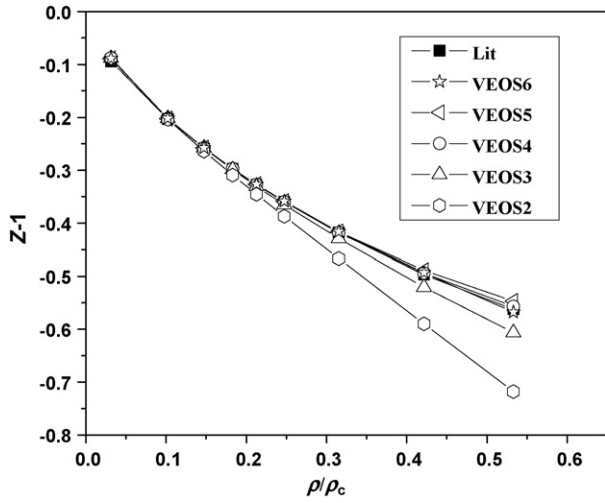


Fig. 11. Plot of reduced Boyle temperature,  $T_B^*/T_c^*$  as a function of well extent for SW fluids.



**Fig. 12.** Deviation from ideality along the saturated vapor line of SW fluid at  $\lambda = 1.5$ . Filled symbol correspond to data due to GC-TMMC simulation [12] and open symbol corresponds to different truncated virial EOS.

### 3.3. PVT behavior

In this part, we examine the ability of different truncated virial EOS to predict the PVT behavior along the saturated vapor line. We compare the predictions of second, third, fourth, fifth and sixth-order truncated virial EOS with molecular simulation data [12] available in the literature.

Figs. 12–14 present the plots of the deviation, based on VEOS, from ideality against reduced density,  $\rho_r = \rho/\rho_c$ , along the saturated vapor line of SW fluids of well widths  $\lambda = 1.5, 1.75$  and  $2.0$ , respectively. Fig. 12 shows that prediction of non-ideality based on VEOS2 is in good agreement (within 2%) with the literature up to the reduced density of 0.15. At higher density, VEOS2 significantly underestimates the pressure value. Inclusion of the third virial coefficient in the virial EOS increases the range of agreement to reduced density of 0.3 as seen in Fig. 12. VEOS4 is in good agreement with the literature data up to reduced density of 0.53 (within 1%). The behavior is not much being affected by the presence of 5th and 6th virial coefficient except that  $B_5$  tend to increase the difference with the literature data. For the current set of density available in the literature, we observed deviation from ideality based on VEOS4 and

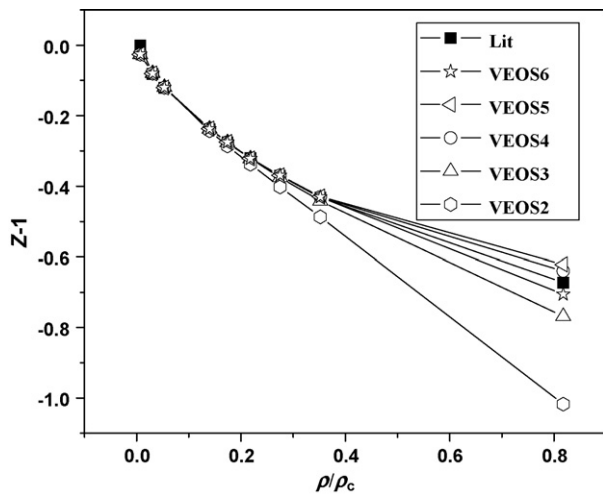


**Fig. 13.** Deviation from ideality along the saturated vapor line of a SW fluid at  $\lambda = 1.75$ . Filled symbol correspond to GC-TMMC simulation [12] and open symbol corresponds to different truncated virial EOS.

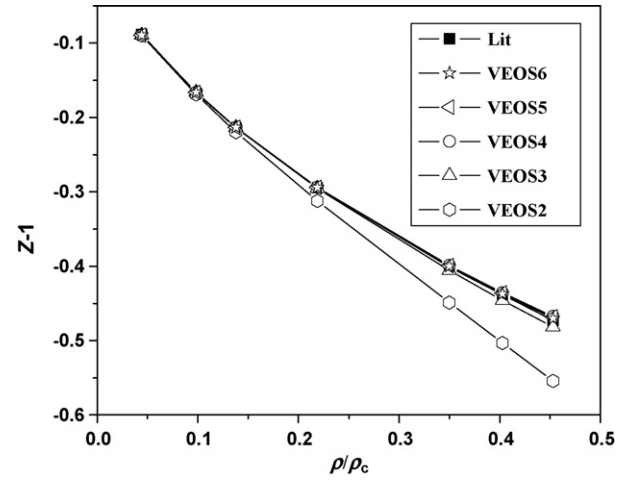


**Fig. 14.** Deviation from ideality along the saturated vapor line of a SW fluid at  $\lambda = 2.0$ . Filled symbol correspond to GC-TMMC simulation [12] and open symbol corresponds to different truncated virial EOS.

VEOS6 to fall within 1% of the literature data. Similar to the above case, VEOS4 and VEOS6 appears to be the best series for the prediction of deviation from ideality for higher well extents as shown in Figs. 13 and 14.

### 3.4. Joule–Thomson coefficient at zero pressure and inversion curves

An additional thermodynamic property of interest is the Joule–Thomson coefficient at zero pressure. This coefficient, as a function of temperature, is often used to estimate the second virial coefficient. These coefficients give insight into inversion temperatures, which are important for throttling processes. The Joule–Thomson coefficient ( $\mu_{JT}$ ) is defined as a derivative of the temperature  $T$  with respect to the pressure  $P$  at constant enthalpy  $h$ :

$$\mu_{JT} = \left( \frac{\partial T}{\partial P} \right)_h, \quad (7)$$

or equivalently, from standard thermodynamic relations:

$$\mu_{JT} = -\frac{1}{C_p} \left( \frac{\partial h}{\partial P} \right)_T, \quad (8)$$

where  $C_p$  is the isobaric heat capacity. Depending on state conditions,  $\mu_{JT}$  may be positive or negative. Positive values imply a cooling of a fluid as it passes through an isenthalpic throttle. The Joule–Thomson coefficient ( $\mu_{JT}$ ) at zero pressure is given by

$$-\varphi^0 \equiv \mu^0 C_p^0 = T \left( \frac{dB_2}{dT} \right) - B_2 \quad (9)$$

where  $C_p^0$  is the zero-pressure value of the molar heat capacity. In this work, we report values of  $(-\varphi^0)$  for square-well fluids of different well widths in Fig. 15. To determine the value of  $dB_2/dT$  from the virial coefficient values obtained via Mayer sampling MC, first we have fitted the virial coefficients data to certain exponential-based functions and then took the derivatives of the fitted functions for  $B_2$ . Joule–Thomson coefficient at zero pressure is positive at low temperature and it decreases exponentially with the increase of the temperature and become negative at extremely high temperature. Increase in the interaction range causes to increase the temperature at which,  $\varphi^0$  approaches zero. For example,  $\lambda = 1.25$ ,  $\varphi^0 = 0$  around  $T^* = 2.57$ , whereas for  $\lambda = 2.0$  this occur at  $T^* = 14.73$ .

Another property of interest is the Joule–Thomson inversion curve, is the locus of points where  $\mu_{JT} = 0$ . The inversion condition

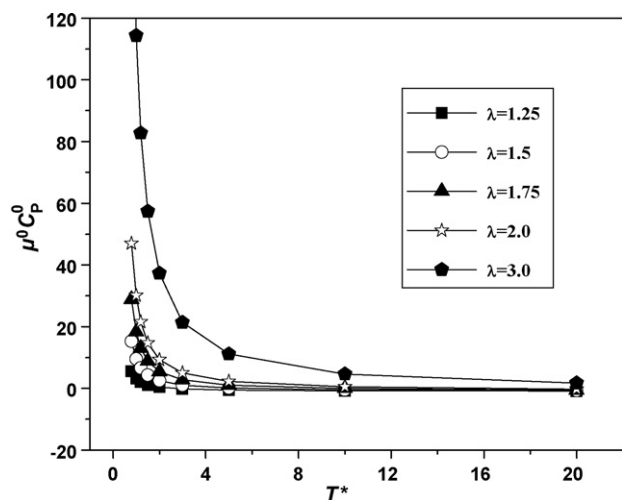


Fig. 15. Joule–Thomson coefficients of square-well fluids at zero pressure as a function of temperature.

[48] is given by equation

$$T \left( \frac{\partial P}{\partial T} \right)_V + V \left( \frac{\partial P}{\partial V} \right)_T = 0 \quad (10)$$

By solving the above equation simultaneously with a given EOS, one can calculate the locus of points for which Joule–Thomson coefficient is zero. Knowledge of the inversion curve is essential for designing throttling processes such as, refrigeration, production of petroleum fluids, etc. Joule–Thomson curve is one of the best criterion to study the behavior of EOS [49,50] in the wide range of temperature and pressure. Inversion curves are usually determined for refrigerants where the knowledge of the region of positive  $\mu_{JT}$  is important. Reservoir fluid abnormalities have been explained by the evaluation of  $\mu_{JT}$  by Kortekass et al. [51].

Until now Joule–Thomson inversion curves are predicted only for few fluids such as Lennard–Jones fluids [52–57], carbon monoxide and carbon dioxide [52,53], certain hydrocarbons [49] such as methane, ethane, ethylene and some mixtures such as natural gas [58]. Figs. 16 and 17 present the predicted Joule–Thomson inversion curves for the LJ and SW fluids, respectively. The predicted inversion curves are based on third (VEOS3), fourth (VEOS4), and

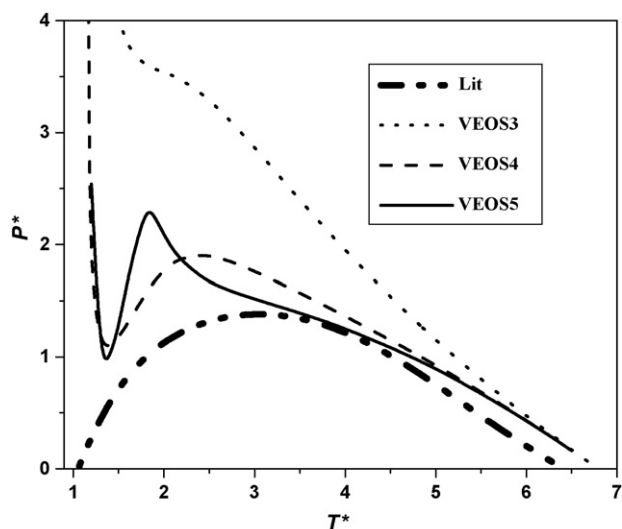


Fig. 16. Joule–Thomson inversion curve of LJ fluid in reduced units predicted from various truncated VEOS and compared with that based on Johnson et al. EOS [59].

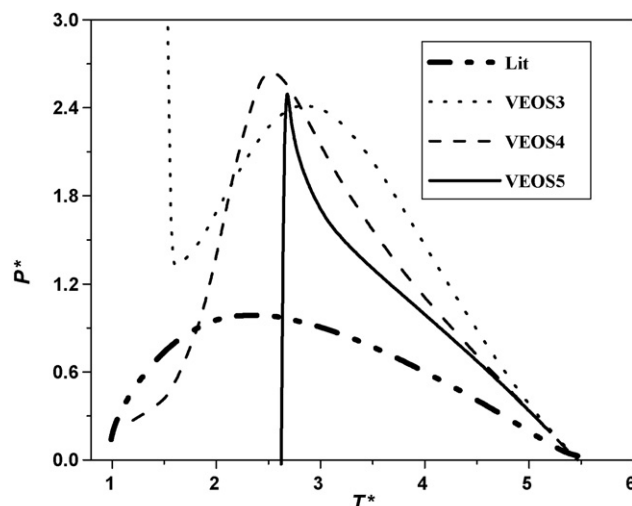


Fig. 17. Joule–Thomson inversion curve of a SW fluid at  $\lambda = 1.5$  in reduced units predicted from various truncated VEOS and compared with that based on Cao et al. EOS [60].

fifth (VEOS5) order truncated virial series and compared with that obtained from respective established EOS for both fluids [59,60]. We do not include VEOS6 due to the numerical difficulty to obtain a solution for inversion curve using Eq. (10). It is evident from Figs. 16 and 17 that VEOS3 is extremely poor for the prediction of inversion curve. With the addition of fourth and fifth virial coefficients, the prediction has improved substantially however; the values still deviate significantly at lower temperatures. Nevertheless, VEOS5 based inversion curve data of LJ are comparable to that of EOS [59] for  $T^* > 3.5$ . On the other hand, for SW fluid of well-width  $\lambda = 1.5$ , the agreement is reasonable with that of EOS [60] for  $T^* > 5.0$ . SW-EOS [60] used in this work is not an exact EOS as the compressibility data due to it deviates significantly from the molecular simulation data. For some cases this deviation is as high as 50%. Nevertheless, VEOS5 lacks the ability to predict inversion curve for a wide range of temperatures. It is yet to be seen the effect of  $B_7$  and higher order coefficients on the prediction of critical properties and the inversion curve, which we plan to study in near future.

#### 4. Conclusions

Mayer sampling based molecular simulation is used to determine values for  $B_2$ – $B_6$  for SW and dimer forming associating fluids. The calculated virial coefficients are in good agreement with available literature data. Virial EOS including these coefficients are developed and used to predict the critical temperature and PVT properties of saturated vapor phase of SW fluids and associating fluid. VEOS4 and VEOS6 do a good job describing the saturated vapor phase of square-well model fluids. Boyle temperature is found to increase with the increase of the well-extent  $\lambda$  and association strength  $\epsilon_{af}$ . Inversion curves predicted from VEOS quantitatively fails to match the ones predicted from established EOS of LJ and SW fluids.

#### Acknowledgements

This work was supported by the Department of Science and Technology (Grant No. SR/S3/CE10/2006) and Department of Atomic Energy, Govt. of India (Grant No. 2006/20/36/05-BRNS).

#### References

- [1] A.J. Masters, J. Phys.: Condens. Matter 20 (2008) 283102.

- [2] D.A. McQuarrie, *Statistical Mechanics*, University Science Books, 2000.
- [3] J.O. Hirschfelder, C.F. Curtiss, R.B. Bird, *Molecular Theory of Gases and Liquids*, John Wiley, New York, 1940.
- [4] J.E. Mayer, M.G. Mayer, *Statistical Mechanics*, 2nd ed., John Wiley & Sons, New York, 1940.
- [5] J.F. Estela-Urbe, J. Jaramillo, *Fluid Phase Equilib.* 231 (2005) 84–98.
- [6] O. Hernández-Garduza, F. García-Sánchez, E. Neaub, M. Rogalski, *J. Chem. Eng.* 79 (2000) 87–101.
- [7] E.M. Holleran, *J. Chem. Thermodyn.* 2 (1970) 779–786.
- [8] K.O. Monago, *Chem. Phys.* 337 (2007) 125–134.
- [9] D.J. Winzor, D.J. Scott, P.R. Wills, *Anal. Biochem.* 371 (2007) 21–25.
- [10] L. Meng, Y.-Y. Duan, *Fluid Phase Equilib.* 258 (2007) 29–33.
- [11] L. Meng, Y.-Y. Duan, L. Li, *Fluid Phase Equilib.* 226 (2004) 109–120.
- [12] J.K. Singh, D.A. Kofke, J.R. Errington, *J. Chem. Phys.* 119 (2003) 3405–3412.
- [13] L. Vega, E. de Miguel, L.F. Rull, G. Jackson, I.A. McLure, *J. Chem. Phys.* 96 (1992) 2296–2305.
- [14] A. Rotenberg, *J. Chem. Phys.* 43 (1965) 1198–1201.
- [15] J.A. Barker, D. Henderson, *Rev. Mod. Phys.* 48 (1976) 587.
- [16] M. Lisal, W.R. Smith, I. Nezbeda, *Fluid Phase Equilib.* 181 (2001) 127–146.
- [17] L. Acedo, A. Santos, *J. Chem. Phys.* 115 (2001) 2805–2817.
- [18] C.P. Bokis, M.D. Donohue, *J. Chem. Phys.* 99 (1995) 12655–12660.
- [19] C. Schultze, M.D. Donohue, *Fluid Phase Equilib.* 158–160 (1999) 229–243.
- [20] H. Adidharma, M. Radosz, *Fluid Phase Equilib.* 161 (1999) 1–20.
- [21] N. Solms, I.A. Kouskoumvekaki, T. Lindvig, M.L. Michelsen, G.M. Kontogeorgis, *Fluid Phase Equilib.* 222–223 (2004) 87–93.
- [22] J.K. Singh, D.A. Kofke, *Phys. Rev. Lett.* 92 (2004) 220601.
- [23] J.K. Singh, D.A. Kofke, *Phys. Rev. Lett.* 94 (2005) 249903.
- [24] S.K. Kwak, D.A. Kofke, *J. Chem. Phys.* 122 (2005) 104508.
- [25] K.M. Benjamin, J.K. Singh, A.J. Schultz, D.A. Kofke, *J. Phys. Chem. B* 111 (2007) 11463–11473.
- [26] L.G. MacDowell, C. Menduina, C. Vega, E. de Miguel, *J. Chem. Phys.* 119 (2003) 11367–11373.
- [27] P.G. Kusalik, F. Liden, I.M. Svishchev, *J. Chem. Phys.* 103 (1995) 10170–10175.
- [28] D. Henderson, O.H. Scalise, W.R. Smith, *J. Chem. Phys.* 72 (1980) 2431.
- [29] M.X. Guo, M. Wang, H. Lu, *Fluid Phase Equilib.* 60 (1990) 221–237.
- [30] K.H. Lee, M.L. Lombardo, S.I. Sandler, *Fluid Phase Equilib.* 21 (1985) 177–196.
- [31] D.M. Heyes, *Mol. Phys.* 69 (1990) 559–569.
- [32] J.R. Elliot, L. Hu, *J. Chem. Phys.* 110 (1999) 3043–3048.
- [33] G. Orkoulas, A.Z. Panagiotopoulos, *J. Chem. Phys.* 110 (1999) 1581–1590.
- [34] S.B. Kiselev, J.F. Ely, L. Lue, J.R. Elliott, *Fluid Phase Equilib.* 200 (2002) 121–145.
- [35] S.B. Kiselev, J.F. Ely, J.R. Elliott, *Mol. Phys.* 104 (2006) 2545–2559.
- [36] J.K. Singh, D.A. Kofke, *J. Chem. Phys.* 121 (2004) 9574–9580.
- [37] S. Wierzchowski, D.A. Kofke, *Fluid Phase Equilib.* 194 (2002) 249–256.
- [38] S. Wierzchowski, D.A. Kofke, *J. Chem. Phys.* 114 (2001) 8752–8762.
- [39] D. Frenkel, B. Smit, *Understanding Molecular Simulation: From Algorithms to Applications*, 2nd ed., Academic Press, 2002.
- [40] D.A. Kofke, *Fluid Phase Equilib.* 41 (2005) 228–229.
- [41] D.A. Kofke, D. Frenkel, *Handbook of Molecular Modeling*, Springer, Netherlands, 2005, p. 683–706.
- [42] D.A. Kofke, B.C. Mihalick, *Fluid Phase Equilib.* 194 (2002) 327–335.
- [43] E.M. Sevicka, P.A. Monson, *J. Chem. Phys.* 94 (1991) 3070–3082.
- [44] S. Katsura, *Phys. Rev.* 115 (1959) 1417–1425.
- [45] Y.A. Vlasov, X.M. You, A.J. Masters, *Mol. Phys.* 100 (2002) 3313–3324.
- [46] C. Menduina, C. McBride, C. Vega, *Phys. Chem. Chem. Phys.* 3 (2001) 1289–1296.
- [47] J. Estrada-Torres, G.A. Iglesias-Silva, M. Ramos-Estrada, K.R. Hall, *Fluid Phase Equilib.* 258 (2007) 148–154.
- [48] J. Corner, *Trans. Farad. Soc.* 39 (1939) 784–791.
- [49] B. Haghighi, M.R. Hussaindokht, M.R. Bozorgmehr, N.S. Matin, *Chin. Chem. Lett.* 18 (2007) 1154–1158.
- [50] N.S. Matin, B. Haghighi, *Fluid Phase Equilib.* 175 (2000) 273–284.
- [51] W.G. Kortekass, C.J. Peters, J. de swaan arons, *Fluid Phase Equilib.* 139 (1997) 207.
- [52] A. Chacin, J.M. Vazquez, E.A. Muller, *Fluid Phase Equilib.* 165 (1999) 147–155.
- [53] C.M. Colina, E.A. Muller, *Int. J. Thermophys.* 20 (1999) 229–235.
- [54] D.M. Heyes, C.M. Llaguno, *Chem. Phys.* 168 (1992) 61–68.
- [55] C.M. Colina, E.A. Muller, *Mol. Simul.* 19 (1997) 237–246.
- [56] F.A. Escobedo, Z. Chen, *Mol. Simul.* 26 (2001) 395–416.
- [57] L.I. Kioupis, G. Arya, E.J. Maginn, *Fluid Phase Equilib.* 200 (2002) 93–110.
- [58] J. Vrabec, A. Kumar, H. Hasse, *Fluid Phase Equilib.* 258 (2007) 34–40.
- [59] J.K. Johnson, J.A. Zollweg, K.E. Gubbins, *Mol. Phys.* 78 (1993) 591–618.
- [60] D. Cao, W. Wang, *Chem. Eng. Sci.* 55 (2000) 2111–2120.
- [61] F. del Rio, E. Avalos, R. Espindola, L.F. Rull, G. Jackson, S. Lago, *Mol. Phys.* 100 (2002) 2531–2546.
- [62] J. Chang, S.I. Sandler, *Mol. Phys.* 81 (1994) 745–765.